NUCLEAR THEORY, Vol. 36 (2017)
eds. M. Gaidarov, N. Minkov, Heron Press, Sofia

Near-Barrier Nucleon Transfer in Reactions ^{3,6}He + ^{45}Sc, ^{197}Au, ^{64}Zn

M.A. Naumenko[1], **V.V. Samarin**[1,2]

[1]Joint Institute for Nuclear Research, 141980 Dubna, Russia
[2]Dubna State University, 141982 Dubna, Russia

Abstract. The theoretical approach based on the numerical solution of the time-dependent Schrödinger equation for neutrons and protons of projectile and target nuclei is applied to the calculation of the cross sections for formation of isotopes ^{44,46}Sc and ^{46}Ti in reaction ^{3}He + ^{45}Sc, ^{46}Sc in reaction ^{6}He + ^{45}Sc, ^{65}Zn in reaction ^{6}He + ^{64}Zn, ^{196,198}Au in reactions ^{3,6}He + ^{197}Au. The neutron (proton) transfer is one of the main reaction channels for the formation of the above-mentioned isotopes in the studied reactions. The contribution of fusion and subsequent evaporation to the experimental data is negligible in the case of ^{6}He + ^{197}Au reaction, whereas in the case of ^{6}He + ^{45}Sc reaction, it is quite large. The fusion-evaporation was taken into account using the NRV evaporation code. Results of calculation demonstrate overall satisfactory agreement with the experimental data. The used implementation of the time-dependent Schrödinger equation method may also be applied to the calculation of reactions with cluster transfer.

1 Introduction

In recent years, the availability of high-intensity beams of radioactive nuclei [1–3] and the progress in accelerator technology have stimulated interest in investigating the properties of helium isotopes and reactions involving such isotopes. The research into low-energy nuclear reactions (*e.g.*, ^{6}He + ^{45}Sc [4], ^{6}He + ^{197}Au [5, 6], ^{6}He + ^{64}Zn [7], and others [8]) provides an opportunity of studying the structure of both ^{3,6}He nuclei and heavy target nuclei.

A ^{3}He nucleus with a low binding energy of 7.7 MeV (here and below the nuclear data are taken from the NRV web knowledge base [9, 10]) is attractive as a tool for investigating the simplest one-neutron transfer processes: stripping (*e.g.*, ^{197}Au(^{3}He, $2p$)^{198}Au, ^{45}Sc(^{3}He, $2p$)^{46}Sc) and pickup (*e.g.*, ^{197}Au(^{3}He, α)^{196}Au, ^{45}Sc(^{3}He, α)^{44}Sc). The possibility of neutron pickup to a single bound state, $1s$, of the ^{4}He nucleus greatly simplifies the picture.

Gamma spectra for similar reactions, *e.g.*, ^{45}Sc(^{3}He, d)^{46}Ti and ^{45}Sc(^{3}He, p)^{47}Ti, measured at certain angles also contain distinct peaks confirming the presence of proton and deuteron transfer [11, 12].

A ^{6}He nucleus can be represented as a three-body system of a tightly bound core (alpha cluster) and two neutrons that form a weakly bound cluster (dineu-

tron) [13–16]. The low neutron separation energy for ^{6}He (0.975 MeV for two neutrons and 1.865 MeV for one neutron [9, 10]) determines the extended nature of neutron distribution (the so-called halo). This halo and the cluster structure can affect elastic scattering, nucleon and cluster transfer processes, nuclear fusion, and breakup reactions.

In this work, the primary channels of the formation of isotopes in the indicated reactions (neutron (proton) transfer and evaporation of particles from a compound nucleus formed after fusion) are analyzed. The cross sections of the formation of evaporation residues are determined using the computational code of the NRV web knowledge base [9, 10].

The distorted wave Born approximation (DWBA; *e.g.*, [9, 10, 17]), the time-dependent Hartree-Fock (TDHF) method (*e.g.*, [18]), Langevin equations (*e.g.*, [19, 20]), and the time-dependent Schrödinger equation (TDSE; *e.g.*, [21–23]) are currently among the most widely used theoretical models and approaches that provide an opportunity of description of nucleon transfer. The DWBA approximation allows one to calculate differential cross sections for specific channels using an exact solution of the Schrödinger equation with phenomenological optical potentials for the relative motion of nuclear cores. However, the use of wave functions of just the initial and the final one-particle (or collective) states in perturbation theory makes it impossible to examine the dynamics of processes. TDHF calculations include the self-consistent quantum motion of all nucleons, but are still performed on relatively coarse meshes with steps of $\sim$0.8 fm [24], which is more than the characteristic distance of probability density oscillations for separate states. Therefore, they can be used only for heavy and intermediate-mass nuclei. In addition, such calculations are time-consuming. Langevin equations including degrees of freedom associated with mass asymmetry (*e.g.*, [19, 20]), are equations of classical mechanics with random forces that include approximate consideration of averaged results of quantum effects. Therefore, they can be used only for heavy and intermediate-mass nuclei. The transfer of individual nucleons in collisions involving light nuclei requires a more accurate quantum description. The method used in this work is based on solving the time-dependent Schrödinger equation [22, 23] and has several advantages over the above techniques. It provides quantum description of several independent outer nucleons (clusters), clear visualization of the dynamics of processes, and fast calculations on a fine mesh (0.1–0.2 fm, which is smaller than the distance of probability density oscillations for separate states), thus allowing us to calculate more accurately the spatial structure of wave functions of nucleons and clusters. In addition, this method can be used for both heavy and light nuclei. Its only drawback is the classical description of motion of nuclei centers.

The aim of this work is description of the experimental data on the formation of isotopes ^{44,46}Sc and ^{46}Ti in reaction ^{3}He + ^{45}Sc, ^{46}Sc in reaction ^{6}He + ^{45}Sc, ^{65}Zn in reaction ^{6}He + ^{64}Zn, ^{196,198}Au in reactions ^{3,6}He + ^{197}Au. The neutron

(proton) transfer is one of the is one of the most important reaction channels for the formation of the above-mentioned isotopes in the studied reactions.

2 Theory

For theoretical description of neutron (proton) transfer during collisions of heavy atomic nuclei we used the time-dependent Schrödinger equation (TDSE) approach [22, 25] for the neutrons (protons) combined with the classical equations of motion of atomic nuclei

$$m_1\ddot{\vec{r}}_1 = -\nabla_{\vec{r}_1} V_{12}\left(|\vec{r}_1 - \vec{r}_2|\right), m_2\ddot{\vec{r}}_2 = -\nabla_{\vec{r}_2} V_{12}\left(|\vec{r}_2 - \vec{r}_1|\right). \qquad (1)$$

Here $\vec{r}_1(t), \vec{r}_2(t)$ are the centers of nuclei with the masses m_1, m_2 and $V_{12}(r)$ is the potential energy of nuclear interaction. We may assume that before contact of the surfaces of spherical nuclei with the radii R_1, R_2 the potential energy $W(\vec{r}, t)$ of a neutron (proton) is equal to the sum of its interaction energies with both nuclei.

The evolution of the components Ψ_1, Ψ_2 of the spinor wave function $\Psi(\vec{r}, t)$ for the neutron (proton) with the mass m during the collision of nuclei is determined by (2) with the operator of the spin-orbit interaction $\hat{V}_{LS}(\vec{r}, t)$

$$i\hbar\frac{\partial}{\partial t}\Psi(\vec{r}, t) = \left\{-\frac{\hbar^2}{2m}\Delta + W(\vec{r}, t) + \hat{V}_{LS}(\vec{r}, t)\right\}\Psi(\vec{r}, t). \qquad (2)$$

The initial conditions for the wave functions were obtained based on the shell model calculations with the parameters providing neutron (proton) separation energies close to the experimental values. An example of the proton levels for the projectile nucleus ^{3}He and the product of the proton transfer reaction, ^{46}Ti nucleus, formed in the collision ^{3}He + ^{45}Sc is shown in Figure 1.

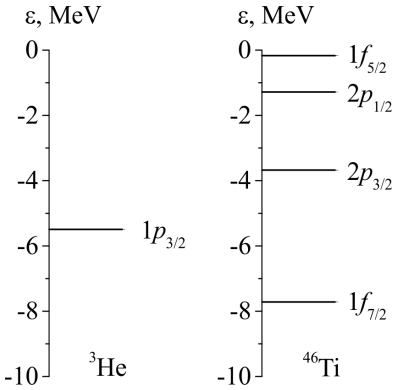

Figure 1. Proton levels for the projectile nucleus ^{3}He and the product of the proton transfer reaction, ^{46}Ti nucleus.

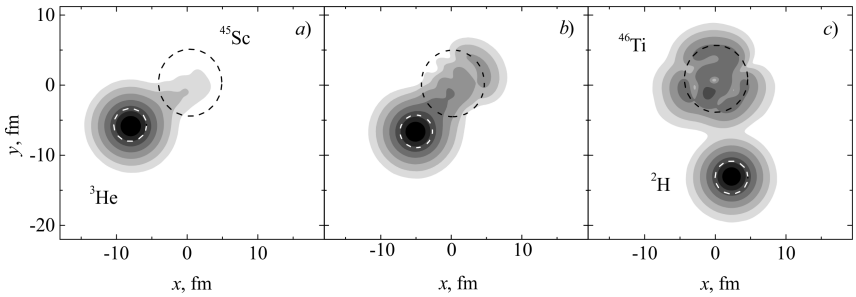

Figure 2. An example of the evolution of the probability density for the proton of ^{3}He nucleus in the collision with ^{45}Sc at $E_{\rm cm} = 10$ MeV and impact parameter $b = 5$ fm. The radii of circumferences equal the effective radii of nuclei. The course of time corresponds to the panel locations (*a*, *b*, *c*).

An example of the evolution of probability density for the proton of ^{3}He nucleus in the collision with ^{45}Sc at $E_{\rm cm} = 10$ MeV and impact parameter $b = 5$ fm is shown in Figure 2. In the calculation, the long range of the Coulomb interaction for protons was taken into account by choosing the large initial distance between the colliding nuclei.

The solution of the time-dependent Schrödinger equation provides the neutron (proton) transfer probability $p\,(b, E)$, where b is an impact parameter and E is the center-of-mass energy. The probabilities for the proton stripping from the ^{3}He in the reaction ^{45}Sc(^{3}He, d)^{46}Ti at the energy $E_{\rm cm} = 8$–25 MeV are shown in Figure 3*a*. For the trajectories with the minimum distance between the nuclei $R_{\rm min}$ the probability was smoothed by the linear dependence

$$p(b, E) \approx \exp\left[A(E) - B(E)R_{\rm min}(b, E)\right]. \qquad (3)$$

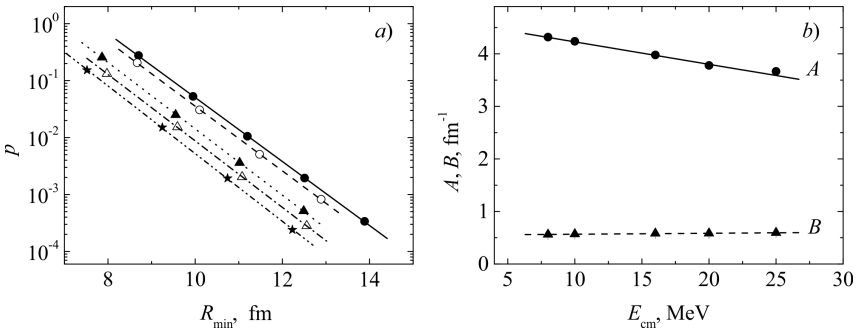

Figure 3. (*a*) The total probability for the proton stripping from the ^{3}He in the reaction ^{45}Sc(^{3}He, d)^{46}Ti at the energy $E_{\rm cm} = 8$ MeV (solid circles), 10 MeV (empty circles), 16 MeV (solid triangles), 20 MeV (empty triangles), 25 MeV (stars). (*b*) The linear regression parameters A and B of the smoothing dependence $p(b, E)$.

The obtained linear regression parameters A and B of the smoothing dependence $p(b, E)$ are shown in Figure 3*b*.

The transfer cross section was calculated as

$$\sigma(E) = \int_0^\infty p(b, E)\, bdb. \tag{4}$$

In the analysis of experimental cross sections for formation of isotopes one must also take into account the possibility of their formation via fusion of colliding nuclei with the subsequent evaporation of nucleons and α-particles. For this purpose we used the computational code of the statistical model available in the NRV web knowledge base [9, 10].

3 Results and Discussion

3.1 ^{3}He + ^{45}Sc

The ^{46}Ti formation cross section in the reaction ^{3}He + ^{45}Sc is shown in Figure 4. Due to the low charge of the formed compound nucleus, the cross section for the fusion with the subsequent evaporation of $1p1n$ is high enough and is comparable with proton stripping cross section. It should be mentioned that in reactions ^{3}He + ^{197}Au, ^{3}He + ^{194}Pt [11] the transfer cross sections are higher than the cross section of fusion with the subsequent $1p1n$ evaporation. Angular distributions were measured and DWBA calculations for proton transfer in three reactions (^{3}He, d) were made in Refs. [11, 26, 27].

Comparison of theoretical calculations with experimental cross sections for formation of isotopes ^{44}Sc and ^{46}Sc in reaction ^{3}He + ^{45}Sc is shown in Figure 5*a* and Figure 5*b*, respectively. Due to the low charge of the formed compound nucleus, the cross sections for the fusion with the subsequent evaporation of

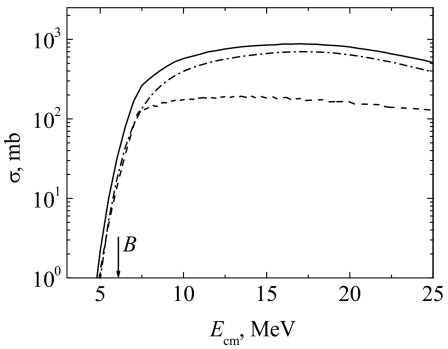

Figure 4. ^{46}Ti formation cross section in the reaction ^{3}He + ^{45}Sc via the following channels: proton stripping (dashed line), fusion-$1p1n$-evaporation (dash-dotted line), and their sum (solid line). Here and below arrows indicate the position of the Coulomb barrier.

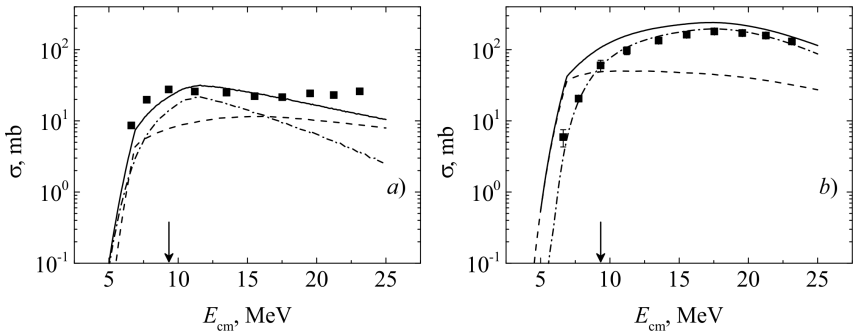

Figure 5. The cross sections for formation of isotopes ^{44}Sc (*a*) and ^{46}Sc (*b*) in reaction ^{3}He + ^{45}Sc. Symbols are the experimental data from Refs. [2, 3], dash-dotted curves are the results of calculation of fusion-α-evaporation (*a*) and fusion-2p-evaporation (*b*) within the NRV web knowledge base [9,10], dashed curves are the results neutron transfer calculations within the TDSE approach, solid curves are the sums of the corresponding transfer and fusion-evaporation channels.

an α-particle and $2p$ are high enough, and are respectively comparable with neutron pickup (^{44}Sc, Figure 5*a*) and stripping (^{46}Sc, Figure 5*b*) cross sections. The corresponding sums of neutron transfer and fusion-evaporation channels provide overall satisfactory agreement of calculation results with experimental data.

3.2 ^{3}He + ^{197}Au

The experimental data on the formation of isotopes ^{196}Au and ^{198}Au in the reaction ^{3}He + ^{197}Au [5,28] are compared to the theoretical calculations in Figure 6*a* and Figure 6*b*, respectively. The cross section for formation of the isotope ^{196}Au via fusion with the subsequent evaporation of an α-particle from the compound nucleus at energies above the Coulomb barrier is substantially (about two orders of magnitude) lower than the experimental data because the high Coulomb barrier prevents the emission of the α-particle from the compound nucleus with the high charge. Formation of ^{198}Au via fusion with the evaporation of $2p$ from the compound nucleus was not observed in calculations. The calculated neutron pickup (^{196}Au, Figure 6*a*) and stripping (^{198}Au, Figure 6*b*) cross sections are in satisfactory agreement with the experimental data.

3.3 ^{6}He + ^{45}Sc, ^{6}He + ^{64}Zn

Comparison of experimental data on the formation of isotopes ^{46}Sc in reaction ^{6}He + ^{45}Sc and ^{65}Zn in reaction ^{6}He + ^{64}Zn with the theoretical calculations is shown in Figure 7*a* and Figure 7*b*, respectively. The cross sections for the formation of the isotopes ^{46}Sc and ^{65}Zn via fusion with the subsequent evaporation of αn is significant at energies above the Coulomb barriers due to the

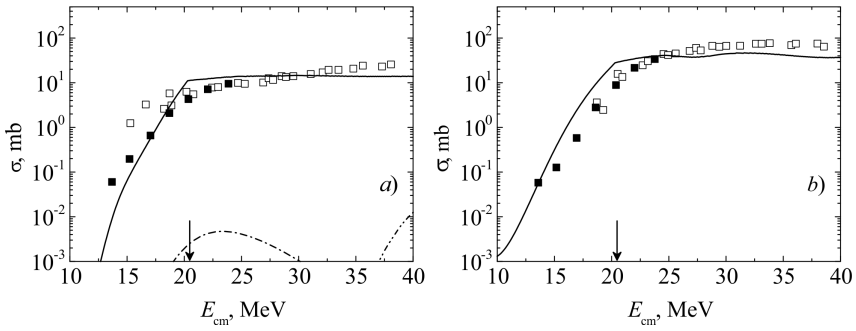

Figure 6. The cross sections for formation of isotopes ^{196}Au (*a*) and ^{198}Au (*b*) in reaction ^{3}He + ^{197}Au. Symbols are the experimental data from Ref. [5] (filled squares) and Ref. [28] (empty squares), dash-dotted and dash-dot-dotted curves are respectively the results of calculation of fusion-α-evaporation and fusion-$2p2n$-evaporation within the NRV web knowledge base [9, 10], solid curves are the results neutron transfer calculations within the TDSE approach.

low charge of the formed compound nucleus. In both cases the corresponding sums of neutron transfer (stripping) and fusion-evaporation channels provide a satisfactory agreement between the calculated results and the experimental data.

3.4 ^{6}He + ^{197}Au

Comparison of experimental data on the formation of isotopes ^{196}Au and ^{198}Au in the reaction ^{6}He + ^{197}Au with the theoretical calculations is shown in Fig-

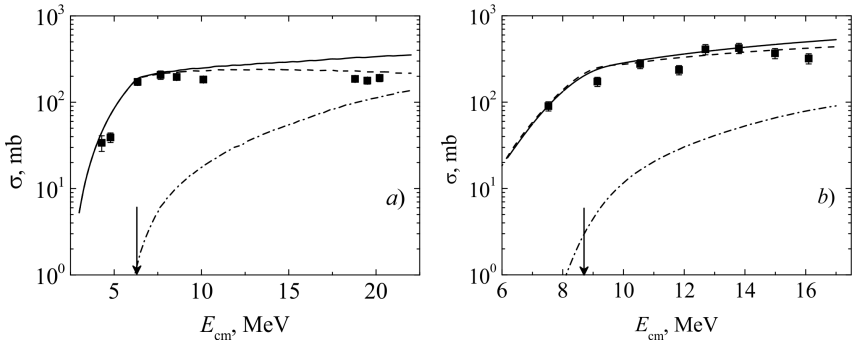

Figure 7. The cross sections for formation of isotopes ^{46}Sc in reaction ^{6}He + ^{45}Sc (*a*) and ^{65}Zn in reaction ^{6}He + ^{64}Zn (*b*). Symbols are the experimental data from Ref. [4] (*a*) and Ref. [7] (*b*), dash-dotted curves are the results of calculation of fusion-αn-evaporation within the NRV web knowledge base [9,10], dashed curves are the results neutron transfer calculations within the TDSE approach, solid curves are the sums of the corresponding transfer and fusion-evaporation channels.

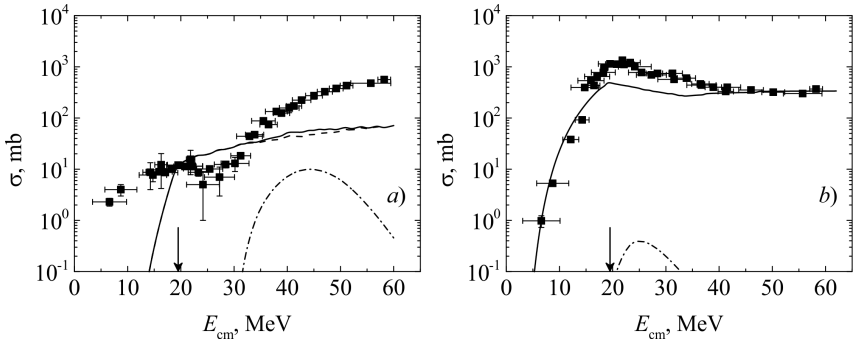

Figure 8. The cross sections for formation of isotopes ^{196}Au (*a*) and ^{198}Au (*b*) and in reaction ^{6}He + ^{197}Au. Symbols are the experimental data from Ref. [6], dash-dotted curves are the results of calculation of fusion-$\alpha 3n$-evaporation (*a*) and fusion-αn-evaporation (*b*) within the NRV web knowledge base [9, 10], dashed curves are the results neutron transfer calculations within the TDSE approach, solid curves are the sums of the corresponding transfer and fusion-evaporation channels.

ure 8*a* and Figure 8*b*, respectively. It can be seen that in this case the contribution of fusion with the subsequent evaporation to the experimental data is negligible due to the high Coulomb barrier of the formed compound nucleus preventing the evaporation of α-particles. It should be mentioned that the yield of isotope ^{198}Au in the reaction ^{6}He + ^{197}Au has already been studied earlier in Ref. [22], but the possible contribution of the fusion-evaporation channel was not evaluated. It is an interesting fact that the experimental yield of the isotope ^{196}Au in the higher-energy region is comparable and even exceeds the yield of the isotope ^{198}Au. Theoretical underestimation of the ^{196}Au cross section compared to the experimental data at higher energies may be explained by not taking into account the processes of knock-out of neutrons from ^{197}Au by the ^{6}He nucleus, as well as the contributions of other reaction mechanisms. In particular, one or two neutrons from ^{6}He may be captured by ^{197}Au followed by evaporation of two or three neutrons, thus resulting in formation of isotope ^{196}Au in the outgoing channel. Accurate theoretical description of such processes is only possible within the solution of fully quantum many-body problem, which is associated with high mathematical complexity and requires a lot of computing power. Thus, this phenomenon requires further theoretical and experimental study.

4 Conclusions

Studying neutron stripping to the excited states of a target nucleus and neutron pickup from its outer and inner shells can yield information on properties of nuclear states of predominantly single-particle (neutron) nature. Experimental data on cross sections for the formation of particular isotopes can be used to

verify theoretical models of neutron (proton) transfer, fusion, and preequilibrium processes.

For the analysis of cross sections for formation of isotopes ^{44,46}Sc and ^{46}Ti in reaction ^{3}He + ^{45}Sc, ^{46}Sc in reaction ^{6}He + ^{45}Sc, ^{65}Zn in reaction ^{6}He + ^{64}Zn, ^{196,198}Au in reactions ^{3,6}He + ^{197}Au the time-dependent Schrödinger equation method for calculation of neutron (proton) transfer cross sections was combined with the statistical model approach using the computational code of the NRV web knowledge base. The sums of neutron transfer and fusion-evaporation channels provided overall satisfactory agreement of calculation results with experimental data. The method may also be applied for calculation of transfer cross sections of clusters (*e.g.*, α-clusters).

Acknowledgements

Authors thank Yu.E. Penionzhkevich, N.K. Skobelev, A.S. Denikin, and A.V. Karpov for fruitful discussions. The work was supported by Russian Science Foundation (RSF), grant No. 17-12-01170.

References

[1] Yu.E. Penionzhkevich, *Phys. Atom. Nucl.* **74** (2011) 1615-1622.

[2] N.K. Skobelev, A.A. Kulko, Yu.E. Penionzhkevich, E.I. Voskoboinik, V. Kroha, V. Burjan, Z. Hons, J. Mrázek, Š. Piskoř, and E. Šimečková, *Phys. Part. Nucl. Lett.* **10** (2013) 410-414.

[3] N.K. Skobelev, A.A. Kulko, Yu.E. Penionzhkevich, E.I. Voskoboinik, V. Kroha, V. Burjan, Z. Hons, J. Mrázek, Š. Piskoř, and E. Šimečková, *Bull. Russ. Acad. Sci.: Phys.* **77** (2013) 795-799.

[4] N.K. Skobelev, A.A. Kulko, V. Kroha, V. Burjan, Z. Hons, A.V. Daniel, N.A. Demekhina, R. Kalpakchieva, A. Kugler, J. Mrázek, Yu.E. Penionzhkevich, Š. Piskoř, E. Šimečková, and E.I. Voskoboynik, *J. Phys. G: Nucl. Part. Phys.* **38** (2011) 035106.

[5] N.K. Skobelev, Yu.E. Penionzhkevich, E.I. Voskoboinik, V. Kroha, V. Burjan, Z. Hons, J. Mrázek, Š. Piskoř, E. Šimečková, and A. Kugler, *Phys. Part. Nucl. Lett.* **11** (2014) 114-120.

[6] Yu.E. Penionzhkevich, R.A. Astabatyan, N.A. Demekhina, G.G. Gulbekian, R. Kalpakchieva, A.A. Kulko, S.M. Lukyanov, E.R. Markaryan, V.A. Maslov, Yu.A. Muzychka, Yu.Ts. Oganessian, R.V. Revenko, N.K. Skobelev, Yu.G. Sobolev, D.A. Testov, and T. Zholdybaev, *Eur. Phys. J. A* **31** (2007) 185-194.

[7] V. Scuderi, A. Di Pietro, P. Figuera, M. Fisichella, F. Amorini, C. Angulo, G. Cardella, E. Casarejos, M. Lattuada, M. Milin, A. Musumarra, M. Papa, M.G. Pellegriti, R. Raabe, F. Rizzo, N. Skukan, D. Torresi, and M. Zadro, *Phys. Rev. C* **84** (2011) 064604.

[8] Y. Nagame, Y. Nakamura, M. Takahashi, K. Sueki, and H. Nakahara, *Nucl. Phys. A* **486** (1988) 77-90.

[9] V.I. Zagrebaev, A.S. Denikin, A.V. Karpov, A.P. Alekseev, M.A. Naumenko, V.A. Rachkov, V.V. Samarin, and V.V. Saiko, *NRV web knowledge base on low-energy*

nuclear physics [online knowledge base], URL: `http://nrv.jinr.ru/` [cited 29 September 2017].

[10] A.V. Karpov, A.S. Denikin, M.A. Naumenko, A.P. Alekseev, V.A. Rachkov, V.V. Samarin, V.V. Saiko, and V.I. Zagrebaev, *Nucl. Instrum. Methods Phys. Res. Sect. Accel. Spectrometers Detect. Assoc. Equip.* **859** (2017) 112-124.

[11] R.W. Barnard and G.D. Jones, *Nucl. Phys. A* **111** (1968) 17-38.

[12] M.N. Rao, J. Rapaport, T.A. Belote, and W.E. Dorenbusch, *Nucl. Phys. A* **151** (1970) 351-368.

[13] Yu.Ts. Oganessian, V.I. Zagrebaev, and J.S. Vaagen, *Phys. Rev. C* **60** (1999) 044605.

[14] V.I. Kukulin, V.M. Krasnopol'sky, V.T. Voronchev, and P.B. Sazonov, *Nucl. Phys. A* **453** (1986) 365-388.

[15] L.I. Galanina and N.S. Zelenskaya, *Phys. Atom. Nucl.* **65** (2002) 1282-1287.

[16] V.V. Samarin and M.A. Naumenko, *Bull. Russ. Acad. Sci.: Phys.* **80** (2016) 283-289.

[17] P.J.A. Buttle and L.J.B. Goldfarb, *Nucl. Phys.* **78** (1966) 409-432.

[18] C. Simenel, *Eur. Phys. J. A* **48** (2012) 152.

[19] V.I. Zagrebaev, M.A. Naumenko, and W. Greiner, *Bull. Russ. Acad. Sci.: Phys.* **69** (2005) 1769-1777.

[20] V.I. Zagrebaev and W. Greiner, *J. Phys. G: Nucl. Part. Phys.* **34** (2007) 1.

[21] V.I. Zagrebaev and V.V. Samarin, *Phys. Atom. Nucl.* **70** (2007) 1003-1016.

[22] V.V. Samarin and K.V. Samarin, *Bull. Russ. Acad. Sci.: Phys.* **76** (2012) 450-453.

[23] V.V. Samarin, *Phys. Atom. Nucl.* **78** (2015) 128-141.

[24] K. Sekizawa and K. Yabana, *Phys. Rev. C* **93** (2016) 054616.

[25] M.A. Naumenko, V.V. Samarin, Yu.E. Penionzhkevich, and N.K. Skobelev, *Bull. Russ. Acad. Sci.: Phys.* **80** (2016) 264-272.

[26] R.W. Barnard and G.D. Jones, *Nucl. Phys. A* **108** (1968) 641-654.

[27] N. Blasi, R. Bijker, M.N. Harakeh, Y. Iwasaki, W.A. Sterrenburg, S.Y. Van Der Werf, and M. Vergnes, *Nucl. Phys. A* **388** (1982) 77-92.

[28] Y. Nagame, K. Sueki, S. Baba, and H. Nakahara, *Phys. Rev. C* **41** (1990) 889-897.